

Quantum Localization in Incommensurate Tight-Binding Chains

C. J. Dyrseth* and K. V. Samokhin

Department of Physics, Brock University, St. Catharines, Ontario L2S 3A1, Canada

(Dated: October 24, 2025)

We explore quantum localization phenomena in a system of two coupled tight-binding chains with incommensurate periods. Employing the inverse participation ratio as a measure of localization, we investigate the effects of geometric incommensurability and external magnetic fields. Numerical results reveal the existence of a mobility edge in the spectrum characterized by an abrupt onset of localization in higher-energy states. We find that localization tends to be enhanced by a weak magnetic field, whereas a strong field delocalizes most states.

I. INTRODUCTION

Electronic properties of disordered and quasi-periodic materials have long been the focus of extensive research in condensed matter physics. In periodic crystals, where atoms are arranged in regular, repeating patterns, the wave function can be expressed as the product of a plane wave and a function with the same periodicity as the lattice, a result known as Bloch's theorem [1]. Physically, this implies that the probability distribution of the electron is spread evenly throughout the lattice. However, in disordered or quasi-periodic materials, this result does not hold. In such systems, it is possible for the wave functions of electrons to become localized.

One of the first theoretical frameworks developed to study disordered materials is the Anderson model [2–4]. In this model, the transfer of electrons between nearest-neighbor sites of a crystal lattice is described using the tight-binding approximation [5, 6], while the on-site energies are randomly selected from a specified range, with the extent of this range referred to as the disorder strength. In one dimension (1D), all electronic states become exponentially localized regardless of the disorder strength [7]. Various methods have been employed to analyze the Anderson model, including the transfer matrix methods [8], Green's function techniques [9], and numerical simulations such as exact diagonalization and the Lanczos algorithm [10]. These techniques calculate key physical quantities such as the localization length, density of states, and conductivity. Experimental validations of the Anderson model have been conducted using ultra-cold atom systems [11] and photonic lattices [12].

Localization in disordered systems usually tends to be suppressed by an external magnetic field. For instance, weakly localized systems in two dimensions (2D) exhibit negative magnetoresistance due to a reduction of constructive interference of the electronic wave functions caused by an additional magnetic phase shift [13]. In the 2D Anderson model, a weak magnetic field reduces localization for states near the Landau band centers [14].

A different class of systems, which are not randomly

disordered but still lack perfect lattice periodicity, are quasi-periodic crystals. One of the most popular quasi-periodic 1D models is the Aubry-André (AA) model [15–17], which features periodically varying on-site energies with the period incommensurate with the lattice, meaning the ratio between the two periods is irrational. In the AA model, all states become localized when the potential strength exceeds a certain threshold. The model is closely related to the Harper model, which describes electrons in a two-dimensional periodic lattice under a uniform magnetic field; the Harper equation can be mapped onto the AA model [18]. The AA model can also be used to describe ultracold atoms in two incommensurate optical lattices. An experimental demonstration of the localization of bosonic atoms in such a system was reported in Ref. [19], offering direct evidence of the AA model predictions. Further experiments have investigated many-body localization in quasi-periodic systems [20].

Several models related to the AA model have been proposed to explore more complex localization phenomena in quasi-periodic systems. One such model is the Soukoulis–Economou model [21], which introduces an additional potential term that breaks the self-duality of the original AA model. This modification allows the coexistence of both extended and localized states within the same system, separated by a mobility edge—critical energy value marking the transition between extended and localized behavior. Mobility edges have also been found theoretically in numerous other generalizations of the single-chain AA model [22–29]. Experimental evidence of a mobility edge in a 1D quasiperiodic optical lattice has been reported in Ref. [30].

The Fibonacci chain [31–34] provides yet another important example. In this 1D tight-binding model, the on-site potentials or hopping amplitudes follow a deterministic, quasi-periodic pattern based on the Fibonacci sequence. The resulting wavefunctions are critical, i.e. neither fully extended nor exponentially localized, instead decaying algebraically and exhibiting self-similar, fractal features. Interestingly, it has been shown that the AA model and the Fibonacci quasi-crystal are topologically equivalent, as one can be smoothly deformed into the other without closing any bulk energy gaps [35].

In this paper, we construct a model of quasi-periodic crystals in which (i) incommensurability naturally arises from the geometry of the system and (ii) it is straightfor-

*E-mail: cd20md@brocku.ca

ward to study the effects of an external magnetic field on quasi-1D localization. Both goals can be achieved if one considers two coupled 1D chains of atoms, with the ratio ρ of the lattice periods being an irrational number. We do not introduce any external on-site potentials, therefore, in contrast to the AA model and its multi-chain generalizations [36–40], the incommensurability in our model affects only the hopping amplitudes.

For numerical analysis, we assume that the chains have different numbers of atoms but the same length, with periodic boundary conditions, and approximate ρ by a ratio of two large coprime numbers. To characterize localization of the electronic wave functions, we use the inverse participation ratio (IPR) [41–43]. The IPR takes values between zero and one, with the larger values corresponding to the more localized wave functions.

The structure of the paper is as follows. In Sec. II we introduce the model of two coupled incommensurate tight-binding chains. In Sec. III we extend the model by including an applied magnetic field. In Sec. IV we describe the numerical method and present the results. In Sec. V we conclude with a discussion of the findings and their implications. A perturbative analysis of the effects of inter-chain hopping for weakly coupled chains is presented in the Appendix. Throughout the paper we use the units in which $c = 1$ and e is the absolute value of the electron charge.

II. THE MODEL

As a minimal model of a geometrically incommensurate 1D system, we consider two coupled chains, A and B , of identical atoms. The chains have the same length, with the numbers of atoms in each chain denoted by N_A and N_B . We assume periodic boundary conditions, so that our system essentially consists of two coupled tight-binding loops, as illustrated in Fig. 1. The circular geometry also allows one to naturally account for all possible hopping terms beyond nearest-neighbor ones. Although we are considering loops, for large enough systems the geometry will appear locally flat.

The loops are vertically separated by a distance d and share the same radius R . The coupling between the chains can be controlled by changing d . In particular, if d is large enough we will have two independent chains. The atoms in each chain are equally spaced along the circumference, with arc lengths between adjacent atoms denoted by a and b for chains A and B , respectively. These arc lengths satisfy the relation $N_A a = N_B b = 2\pi R$, so that one can also control the inter-atomic couplings by varying the number of atoms in each chain.

To model an incommensurate system, we set the ratio

$$\rho = \frac{N_A}{N_B} = \frac{b}{a} \quad (1)$$

to closely approximate an irrational number. This can be

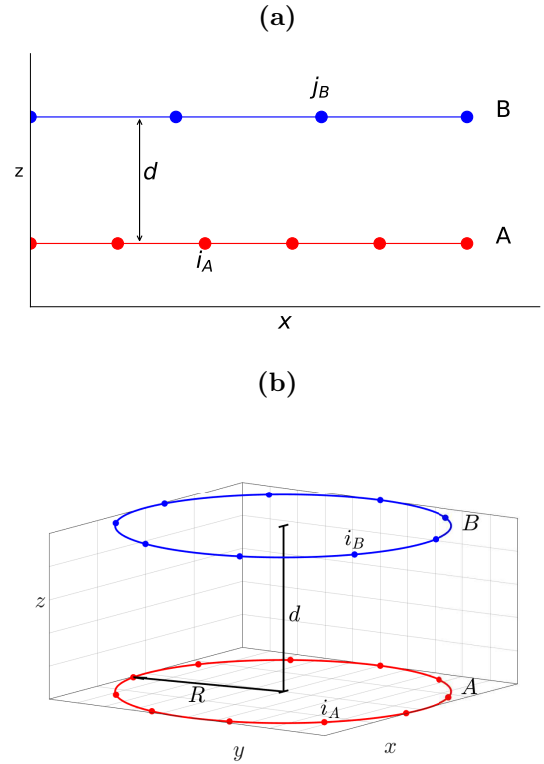


FIG. 1: (Color online) Linear chains with periodic boundary conditions (a), represented by circular chains (b).

achieved using the method of continued fractions [44, 45]. We represent the ratio (1) in the following form:

$$\rho = a_0 + \frac{1}{a_1 + \frac{1}{\ddots + \frac{1}{a_p}}}, \quad (2)$$

where a_0, a_1, \dots, a_p are integers [46]. In our analysis we will try to bring ρ close to the golden ratio $\phi = (1 + \sqrt{5})/2 \simeq 1.618$, which corresponds to all $a_i = 1$ ($i \geq 0$). Truncating this infinite sequence to p terms leads to a rational approximation for ϕ called the p th convergent and denoted as ϕ_p . The latter is given by a ratio of consecutive Fibonacci numbers:

$$\phi_p = \frac{F_{p+1}}{F_p}. \quad (3)$$

The reciprocal of the golden ratio $\phi^{-1} = (\sqrt{5} - 1)/2$, which is obtained by setting $a_0 = 0$ and $a_i = 1$ for $i > 0$, is also often used in the literature on incommensurate models. Using ϕ^{-1} effectively swaps the A and B chains, i.e., $N_A \leftrightarrow N_B$ and $a \leftrightarrow b$.

To develop a tight-binding model of the system, we introduce the position basis defined by the states $|A, i_A\rangle$

and $|B, i_B\rangle$, where $i_A = 1, \dots, N_A$, $i_B = 1, \dots, N_B$ are the indices that label atoms in the chains A and B , respectively. The Hamiltonian consists of three components: intra-chain hopping terms \hat{H}_A and \hat{H}_B , and inter-chain hopping term $\hat{\tilde{H}}$:

$$\hat{H} = \hat{H}_A + \hat{H}_B + \hat{\tilde{H}}. \quad (4)$$

The intra-chain blocks are given by

$$\begin{aligned} \hat{H}_A &= - \sum_{i_A \neq j_A} t_A(i_A, j_A) |A, i_A\rangle \langle A, j_A|, \\ \hat{H}_B &= - \sum_{i_B \neq j_B} t_B(i_B, j_B) |B, i_B\rangle \langle B, j_B|, \end{aligned} \quad (5)$$

where t_A and t_B are the hopping amplitudes within the A and B chains, respectively. The inter-chain blocks are given by

$$\hat{\tilde{H}} = - \sum_{i_A, j_B} \tilde{t}(i_A, j_B) |A, i_A\rangle \langle B, j_B| + \text{H.c.}, \quad (6)$$

where \tilde{t} are the hopping amplitudes between the chains.

In our model, we include the hopping amplitudes between *all* pairs of atoms. Assuming, for simplicity, that there is one isotropic (*s*-wave) orbital per atom, the electron wave functions' overlap for two atoms located at \mathbf{r} and \mathbf{r}' depends only on the distance $|\mathbf{r} - \mathbf{r}'|$. Then, one can write

$$\begin{aligned} t_A(i_A, j_A) &= t \exp\left(-\frac{|\mathbf{r}_A(i_A) - \mathbf{r}_A(j_A)|}{\lambda}\right), \\ t_B(i_B, j_B) &= t \exp\left(-\frac{|\mathbf{r}_B(i_B) - \mathbf{r}_B(j_B)|}{\lambda}\right), \\ \tilde{t}(i_A, j_B) &= t \exp\left(-\frac{|\mathbf{r}_A(i_A) - \mathbf{r}_B(j_B)|}{\lambda}\right), \end{aligned} \quad (7)$$

where t is the hopping constant, which has the dimension of energy, and λ characterizes the spatial extent of the atomic wave functions. The positions of atoms in the chains are given by

$$\begin{aligned} \mathbf{r}_A(i_A) &= R \cos \frac{2\pi i_A}{N_A} \hat{\mathbf{x}} + R \sin \frac{2\pi i_A}{N_A} \hat{\mathbf{y}}, \\ \mathbf{r}_B(i_B) &= R \cos \frac{2\pi i_B}{N_B} \hat{\mathbf{x}} + R \sin \frac{2\pi i_B}{N_B} \hat{\mathbf{y}} + d \hat{\mathbf{z}}, \end{aligned}$$

see Fig. 1b. Therefore, the hopping amplitudes take the following form:

$$\begin{aligned} t_A(i_A, j_A) &= t \exp\left[-\frac{2R}{\lambda} \left| \sin \frac{\pi(i_A - j_A)}{N_A} \right| \right], \\ t_B(i_B, j_B) &= t \exp\left[-\frac{2R}{\lambda} \left| \sin \frac{\pi(i_B - j_B)}{N_B} \right| \right], \end{aligned}$$

$$\begin{aligned} \tilde{t}(i_A, j_B) &= t \exp\left[-\frac{2R}{\lambda} \sqrt{\sin^2\left(\frac{\pi i_A}{N_A} - \frac{\pi j_B}{N_B}\right) + \left(\frac{d}{2R}\right)^2}\right]. \end{aligned} \quad (8)$$

Note that t_A and t_B are invariant with respect to the lattice translations in the respective chains, i.e., depend only on $|i_A - j_A|$ or $|i_B - j_B|$, but have different magnitudes if $N_A \neq N_B$. In contrast, the inter-chain hopping amplitudes are *not* translationally invariant.

Although all possible hopping terms are included in our model, in practice, for any given atom, only a few neighbors in both chains make a non-negligible contribution. The magnitudes of the inter-chain hoppings vary from atom to atom in a quasi-random fashion, producing a “geometrical disorder” in the system. We would like to mention here the study of the energy spectrum in a model of two coupled weakly incommensurate “Moiré chains” [47]. In this model, only the nearest-neighbor intra-chain hopping amplitudes (same in both chains) were considered and a different dependence of the inter-chain hoppings on the distance between the sites was assumed.

A. Effects of magnetic field

We now include the effects of an external magnetic field in our tight-binding model, which can be achieved by using the Peierls substitution [48, 49]. In this method each hopping amplitude in Eqs. (5) and (6) is modified by a complex phase factor: $t_{\mathbf{r}\mathbf{r}'} \rightarrow t_{\mathbf{r}\mathbf{r}'} e^{i\varphi_{\mathbf{r}\mathbf{r}'}}$, where

$$\varphi_{\mathbf{r}\mathbf{r}'} = -\frac{e}{\hbar} \int_{\mathbf{r}}^{\mathbf{r}'} \mathbf{A} \cdot d\mathbf{l}. \quad (9)$$

The integration here is performed along the straight path the electron hops.

Let us first consider an external magnetic field parallel to the chains' plane, i.e. oriented along the z -axis in the circular geometry, $\mathbf{B} = B_{\parallel} \hat{\mathbf{z}}$, see Fig. 2. Using the cylindrical gauge for the vector potential, we have $\mathbf{A} = (B_{\parallel} R/2) \hat{\theta}$. Applying Stokes' theorem, it is straightforward to demonstrate that the line integral in Eq. (9) between sites i and j in the same or different chains is equal to the magnetic flux through the triangular area shown in Fig. 2. Namely,

$$\varphi_{ij} = -\frac{1}{\Phi_0} \int_{S_{\parallel}} \mathbf{B} \cdot d\mathbf{S}, \quad (10)$$

where $\Phi_0 = \hbar/e$ is the magnetic flux quantum. The explicit forms of the phases for intra-chain and inter-chain hopping are given by

$$\varphi(i_A, j_A) = \chi_{\parallel} \frac{N_A}{2\pi} \sin \frac{2\pi(i_A - j_A)}{N_A},$$

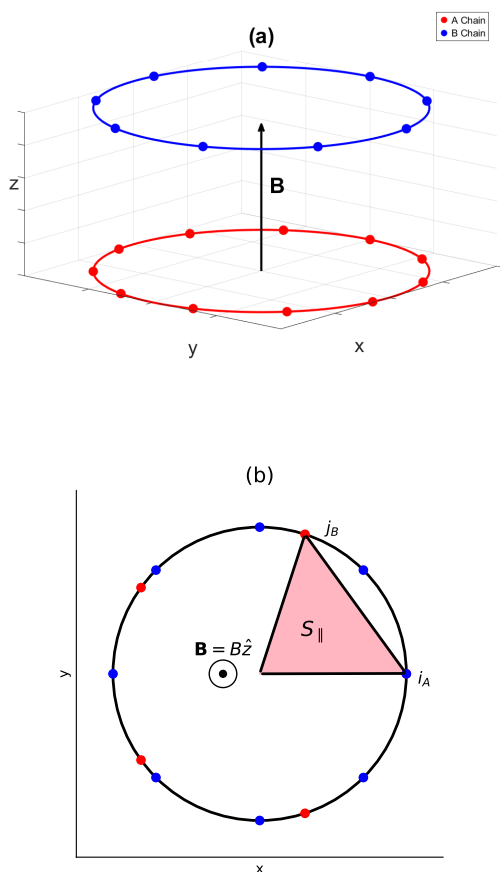


FIG. 2: (Color online) (a) Circular chains with an external magnetic field orientated along the z -axis. (b) The triangular segment we integrate over in Eq. (10). The sites can be in different chains, as shown, or in the same chain.

$$\varphi(i_B, j_B) = \chi_{\parallel} \frac{N_A}{2\pi} \sin \frac{2\pi(i_B - j_B)}{N_B},$$

$$\varphi(i_A, j_B) = \chi_{\parallel} \frac{N_A}{2\pi} \sin \left(\frac{2\pi}{N_A} i_A - \frac{2\pi}{N_B} j_B \right).$$

Here

$$\chi_{\parallel} = \frac{\pi R^2 B_{\parallel}}{N_A \Phi_0}, \quad (11)$$

is the dimensionless magnetic field strength, which will serve as an adjustable parameter in our numerical analysis.

Next, we investigate the effects of a radial magnetic field $\mathbf{B} = B_{\perp} \hat{r}$ on the two tight-binding loops. Note that a purely radial magnetic field would violate Gauss's law for magnetism $\nabla \cdot \mathbf{B} = 0$ and therefore cannot exist in nature. We use this field configuration to approximate two long chains with periodic boundary conditions under a *perpendicular* field as depicted in Fig. 3.

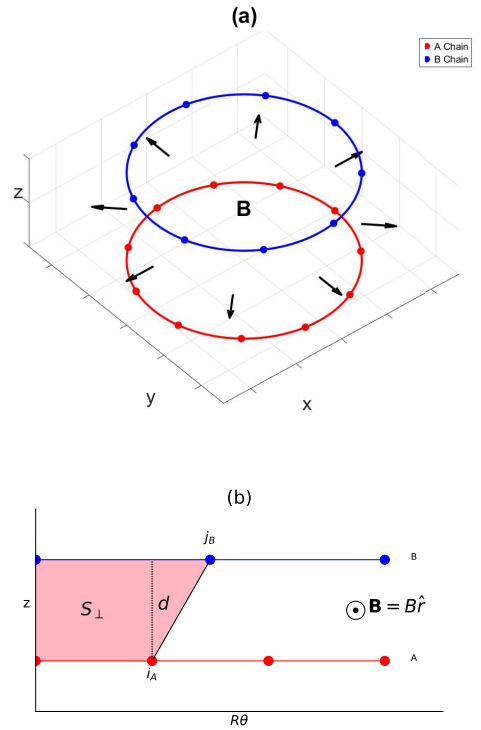


FIG. 3: (Color online) (a) Circular chains with an external magnetic field orientated along the normal of the surface of the cylinder formed by the two chains. (b) The incommensurate chain system in a perpendicular (radial) magnetic field. The shaded area shows the segment we integrate over in Eq. (12).

The vector potential corresponding to the radial field can be chosen as $\mathbf{A} = B_{\perp} R \theta \hat{z}$, where θ is the polar angle in the xy plane. It is easy to see that only the inter-chain hopping amplitudes are affected by a phase factor, which is given by

$$\varphi(i_A, j_B) = -\frac{1}{\Phi_0} \int_{S_{\perp}} \mathbf{B} \cdot d\mathbf{S}. \quad (12)$$

This integral represents the magnetic flux through the shaded area S_{\perp} shown in Fig. 3. The resulting phase factor becomes

$$\varphi(i_A, j_B) = -\chi_{\perp}(i_A + \rho j_B),$$

where

$$\chi_{\perp} = \frac{\pi B_{\perp} R d}{N_A \Phi_0}, \quad (13)$$

is the dimensionless strength of a perpendicular magnetic field.

III. NUMERICAL ANALYSIS

In periodic systems, Bloch's theorem enables analytical calculation of the energy spectrum by assuming extended plane wave solutions for the wave function. The number of atoms per unit cell in a periodic lattice directly corresponds to the number of energy bands [50]. However, our system does not repeat periodically; instead, it consists of $N_A + N_B$ atoms within a single “unit cell”, which coincides with the whole crystal. This non-periodicity means that extended plane-wave solutions are no longer valid and that Bloch's theorem cannot be applied, resulting in $N_A + N_B$ distinct energy levels rather than energy bands. By increasing the size of the system and tuning the ratio ρ to approximate an irrational number, we effectively render the system incommensurate. Since there is no analytical solution available for such a system, we must resort to numerical methods to find the wave functions and energy eigenvalues.

We cannot label the energy levels in terms of the wave vector \mathbf{k} as in a periodic system. Instead, we now label the energy levels from lowest to highest using an integer index $n = 1, \dots, N_A + N_B$. The eigenstates of the Hamiltonian are denoted as $|n\rangle$, and the corresponding energies – as E_n . Measuring the latter in units of the hopping constant t , see Eq. (7), we solve the following eigenvalue problem:

$$\frac{\hat{H}}{t} |n\rangle = E_n |n\rangle, \quad (14)$$

where \hat{H} is given by Eq. (4). The eigenvectors have the following form:

$$|n\rangle = \begin{pmatrix} \psi_n(A, 1) \\ \vdots \\ \psi_n(A, N_A) \\ \psi_n(B, 1) \\ \vdots \\ \psi_n(B, N_B) \end{pmatrix}, \quad (15)$$

with the components $\psi_n(A, i_A) = \langle A, i_A | n \rangle$ and $\psi_n(B, i_B) = \langle B, i_B | n \rangle$. The eigenvectors are normalized:

$$\langle n | n \rangle = \sum_{i_A=1}^{N_A} |\psi_n(A, i_A)|^2 + \sum_{i_B=1}^{N_B} |\psi_n(B, i_B)|^2 = 1.$$

In our model, following a considerable precedent in the previous studies of incommensurate 1D systems [15], we focus on using the golden ratio ϕ as the incommensurability parameter. To better represent real physical systems we select large values for N_A and N_B . By choosing values of N_A and N_B in the thousands, we ensure a high degree of precision in approximating ϕ while maintaining practical relevance for numerical analysis. Namely,

we use

$$\rho = \phi_{17} = \frac{2584}{1597}, \quad (16)$$

as determined from Eq. (3), i.e. set $N_A = F_{18} = 2584$ and $N_B = F_{17} = 1597$, where F_p is the p th Fibonacci number. Selecting higher-order approximations does not qualitatively affect our results.

To facilitate our analysis, we introduce dimensionless parameters that characterize the system's geometric properties. Measuring the lattice constant in the A chain and the vertical spacing between the chains in units of the size of the atomic wave functions (or, in other words, setting the latter to unity for simplicity), we have $a/\lambda \rightarrow a$ and $d/\lambda \rightarrow d$. From Eq. (8), we obtain the dimensionless hopping amplitudes

$$\begin{aligned} t_A(i_A, j_A) &= \exp \left[-\frac{N_A a}{\pi} \left| \sin \frac{\pi(i_A - j_A)}{N_A} \right| \right], \\ t_B(i_B, j_B) &= \exp \left[-\frac{N_B b}{\pi} \left| \sin \frac{\pi(i_B - j_B)}{N_B} \right| \right], \\ \tilde{t}(i_A, j_B) &= \exp \left[-\frac{N_A a}{\pi} \sqrt{\sin^2 \left(\frac{\pi i_A}{N_A} - \frac{\pi j_B}{N_B} \right) + \left(\frac{\pi d}{N_A a} \right)^2} \right], \end{aligned} \quad (17)$$

where we used $N_A a = N_B b$.

As a measure of the wave function's extent over lattice sites we use the IPR, which yields the reciprocal of the count of sites encompassed by the wave function. The IPR of a normalized state $|\psi\rangle$ is defined as [41–43]

$$\text{IPR} = \sum_{i=1}^N |\psi(i)|^4,$$

where $\psi(i) = \langle i | \psi \rangle$ is the value of the wave function at the i^{th} site. In our two-chain model, the above expression takes the form

$$\text{IPR}(n) = \sum_{i_A=1}^{N_A} |\psi_n(A, i_A)|^4 + \sum_{i_B=1}^{N_B} |\psi_n(B, i_B)|^4. \quad (18)$$

The value of the IPR provides valuable insight into the degree of localization of a given quantum state. The IPR trends towards zero (scaling as L^{-1} , where L is the chains' length) for a delocalized wave function, whereas it is equal to unity in the case of a wave function confined to a single lattice site.

IV. RESULTS

In our numerical calculations, we use $N_A = 2584$ and $N_B = 1597$ and diagonalize a 4181×4181 Hamiltonian matrix for different values of the dimensionless lattice

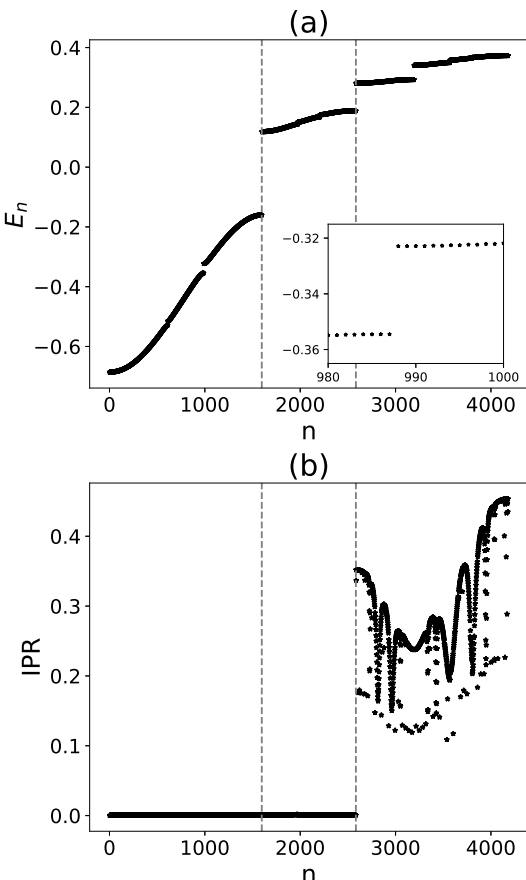


FIG. 4: Data collected from a system with $a = 2$ and $d = 1$. (a) The energy spectrum, ordered from lowest to highest, is plotted over the energy index n ($1 \leq n \leq N_A + N_B$). (b) The IPR plotted over the energy index n . The dashed lines show the locations of large energy gaps at $n = N_B$ and $n = N_A$.

constant a and the inter-chain separation d (the lattice constant in the B chain is given by $b = pa$). The effects of a magnetic field, which are described by the dimensionless parameters χ_{\parallel} and χ_{\perp} , are considered in Sec. IV A.

In Fig. 4, we present the energy spectrum and corresponding values of the IPR for a set of parameters where localization is observed, including a “zoomed in” view of one segment from the energy spectrum. The spectrum comprises discrete energy levels, and notably, it exhibits several gaps that are significantly wider than the typical spacing between adjacent energy levels. It is possible to average our results with respect to the rotation of one of the chains. For instance, we can average with respect to the rotation of the B chain through an angle of 0 to $2\pi/N_A$. However, since this has a negligible impact on our results, we have chosen not to average in this way.

The evolution of the energy spectrum as a function of the inter-chain separation d is shown in Fig. 5. At sufficiently large values of d the spectrum is smooth and agrees with analytical results for decoupled chains. When

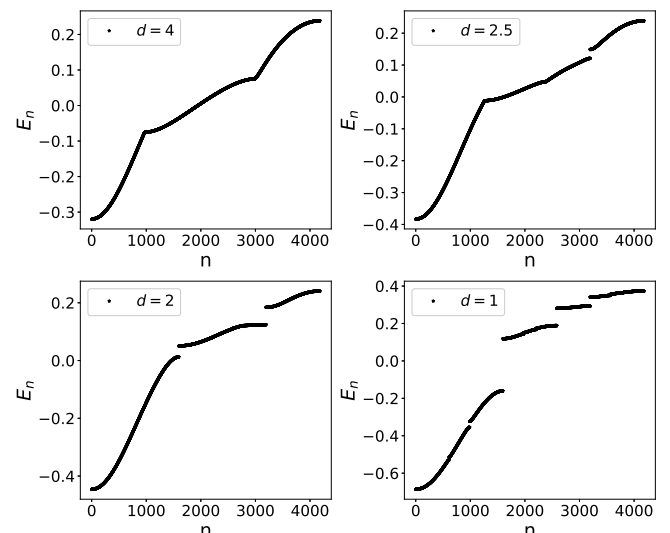


FIG. 5: Evolution of the energy spectrum as the inter-chain separation d is decreased at fixed $a = 2$.

d is decreased, gaps begin to appear in the spectrum. Interestingly, these gaps seem to be located exactly at indices corresponding to the Fibonacci numbers $n = F_p$ or their simple combinations. This can be understood as an effect of “small denominators” in the perturbation expansions with respect to a weak inter-chain coupling, see Appendix A.

The relationship between the IPR and the inter-chain separation is shown in Fig. 6. Qualitatively, there is an inverse relationship between the IPR and d , indicating that as d increases, the IPR decreases. This confirms the intuitive expectation that decoupling the chains by increasing the vertical spacing between them reduces the amount of localization.

Our results for the coupled chains indicate that higher-energy states tend to be localized, exhibiting nonzero values of the IPR, whereas lower-energy states remain extended. Notably, the transition from extended to localized states is not continuous; instead, it is abrupt and coincides with a gap in the energy spectrum. These findings suggest a strong correlation between the presence of energy gaps and the onset of localization in higher-energy states.

To illustrate the shape of the localized states, in Fig. 7 we plot the probability densities $|\psi_n(A, i_A)|^2$ and $|\psi_n(B, i_B)|^2$ using as an example the state with $n = 2750$. The wave function exhibits sharply localized peaks in both chains in close proximity of each other. To characterize its spatial extent, we approximate the probability density in each chain by an exponential function of the form

$$|\psi(\theta)|^2 = |\psi(\theta_0)|^2 \exp\left(-\frac{|\theta - \theta_0|}{\delta}\right), \quad (19)$$

where we use the angular coordinate θ to take advantage

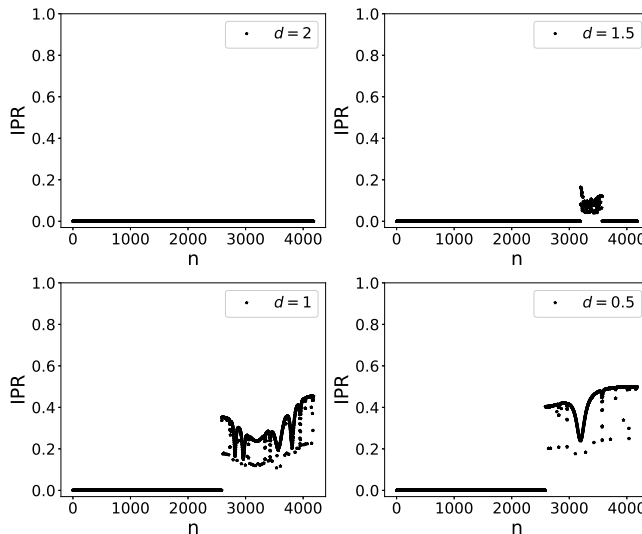


FIG. 6: Evolution of the IPR as the inter-chain separation d is decreased at fixed $a = 2$.

of the cylindrical symmetry of the system. By fitting the numerical data, we can extract the angular localization length δ . In Fig. 7b, we show the results of this procedure for the probability density in the A and B chains separately, thereby determining two distinct localization lengths, δ_A and δ_B . Note that we are not making the claim that the wave functions are exponentially localized based on our data. We use the simple fitting function (19) only to get some qualitative insight into the spatial extent of the localized eigenstates.

It may be more convenient to define a linear localization length $\xi = R\delta$, doing this we can compare the extent of localization to the lattice constant. For the $n = 2750$ state, we find $\xi_A \simeq 0.387a$ and $\xi_B \simeq 0.309b$ (0.499a). Thus the wave function is strongly localized on the scale of the lattice constant.

The dependence of the IPR on the lattice constant a is shown in Fig. 8. We see that increasing a while keeping the inter-chain spacing constant decreases the prevalence of intra-chain hopping relative to inter-chain hopping, which in turn increases the number of localized states.

The percentage P of localized states in the system, for different values of the parameters a and d , is shown in Fig. 9. We define the threshold for localization as $\text{IPR} > (N_A + N_B)^{-1/2}$, i.e. as the geometric mean between the IPRs for a fully extended state, $\text{IPR} = (N_A + N_B)^{-1}$ and a fully localized state, $\text{IPR} = 1$. In the figure, the vertical axis represents d and the horizontal axis represents a , while the red dashed line corresponds to $d = a$. Below the dotted line, inter-chain hopping dominates over intra-chain hopping, whereas above this line, intra-chain hopping is predominant. Notably, all localized states are found below the dotted line.

Many studies have examined the behaviour of wave functions at the transition between localized and extended phases. In the Aubry-André model, for example,

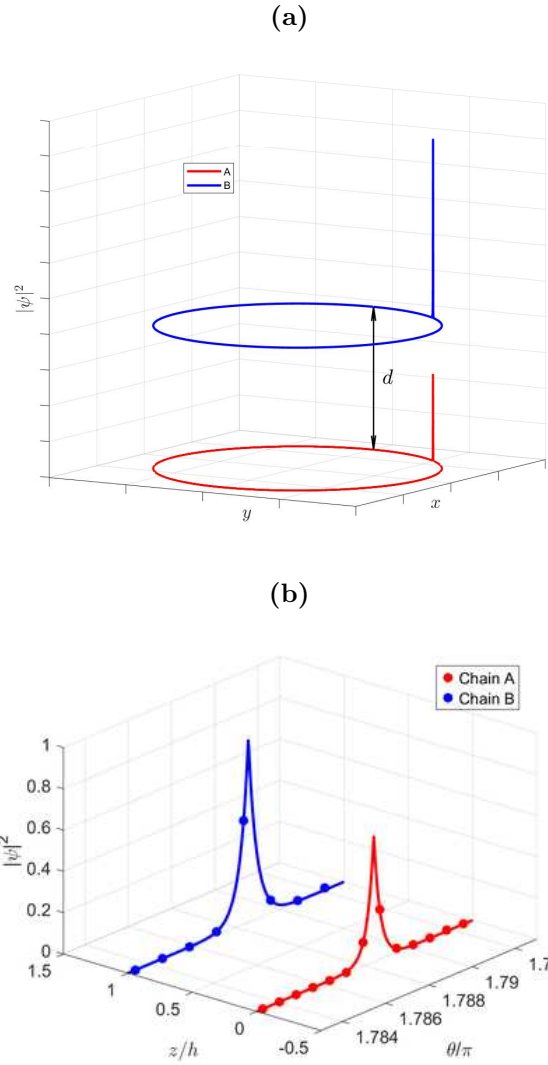


FIG. 7: (Color online) (a) “Bird’s-eye” view of the probability densities $|\psi_n(A, i_A)|^2$ and $|\psi_n(B, i_B)|^2$ in the localized state with $n = 2750$, $a = 2$, and $d = 1$. (b) Close-up view of the same probability densities, using cylindrical coordinates θ and z . Data is approximately fit to Eq. (19).

wave functions at the critical point are neither fully localized nor extended, but exhibit irregular multifractal fluctuations across all length scales [51]. In contrast, our model shows an abrupt transition between localized and extended states, with no intermediate phase. This means that on either side of the mobility edge, the wave functions are either localized or extended, sharing the same properties as other states in their respective phases.

A. Effects of magnetic field

For a magnetic field $\mathbf{B} = B_{\parallel}\hat{\mathbf{z}}$, with the field strength characterized by the parameter (11), we observe no significant qualitative change in the shape of the IPR distri-

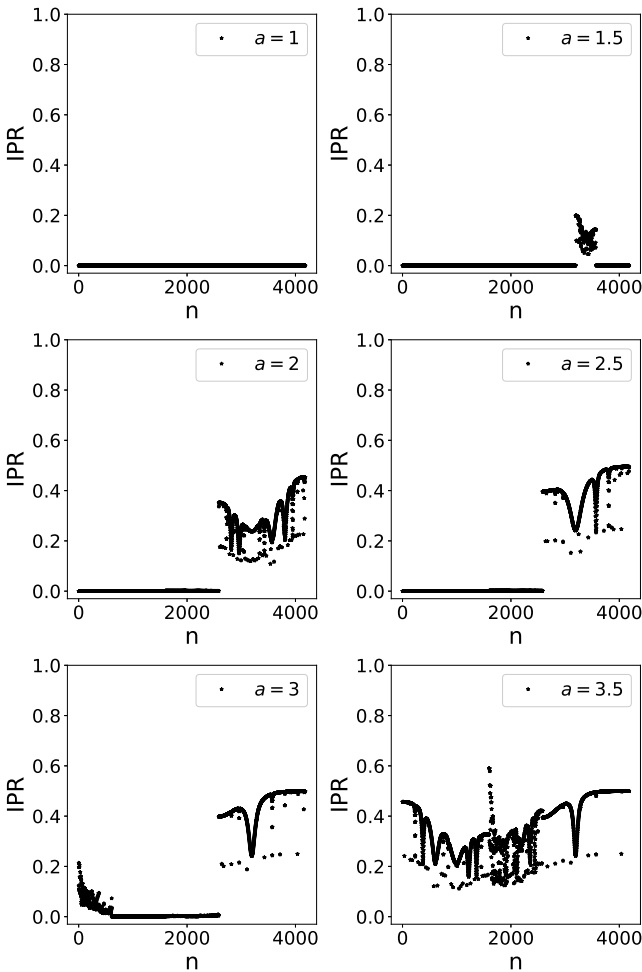


FIG. 8: Dependence of the IPR on the lattice constant a at fixed $d = 1$.

bution for any choice of parameters. This indicates that localization is not affected by this orientation of the field.

In contrast, a magnetic field perpendicular to the plane of the chains, which corresponds to $\mathbf{B} = B_{\perp} \hat{\mathbf{r}}$ in the cylindrical geometry, has a pronounced effect on localization. In Fig. 10 we show the evolution of the IPR as the magnetic field strength, characterized by the parameter (13), increases. Initially, for small fields, the IPR values for some states increase, indicating a strengthening of localization in already localized states and the localization of some previously delocalized sites. However, as the field strength increases further, the majority of IPR values decrease to zero. This suggests that while weak fields can enhance localization in certain states, stronger fields lead to the delocalization of most states. Eventually, all states become delocalized.

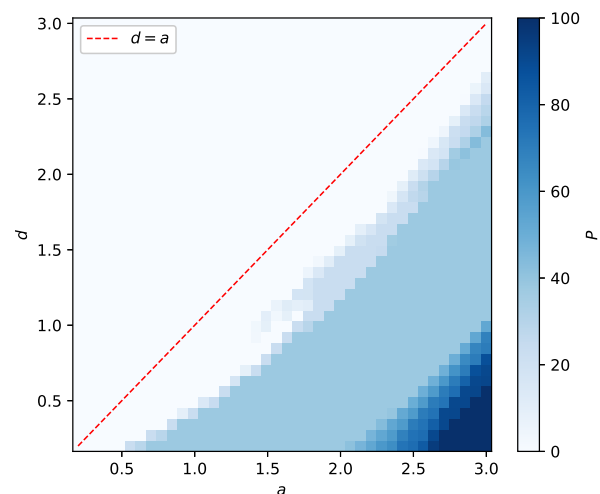


FIG. 9: (Color online) The percentage of localized states, defined by the criterion $\text{IPR} > (N_A + N_B)^{-1/2} \approx 0.0154$, is shown for different values of a and d . The dotted red line marks the boundary between regimes dominated by inter-chain and intra-chain hopping.

V. CONCLUSIONS

In conclusion, we showed that electron states can be localized in a quasi-1D system without disorder, due to inter-chain hopping between two coupled incommensurate chains. In contrast to other models of incommensurate 1D crystals, such as the AA model, we observe the mobility edges separating extended from localized states, which are controlled by the inter-chain separation. These mobility edges are abrupt and coincide with gaps in the energy spectrum. Localization arises when inter-chain hopping dominates intra-chain hopping; however, this dependence is complex and not solely determined by the ratio of the distance between the chains to the lattice constant.

Our model is well suited for studying the effect of a magnetic field on localization, which we found to strongly depend on the field's orientation. A magnetic field parallel to the chains' plane does not alter localization properties. In contrast, a magnetic field perpendicular to the chains' plane enhances localization at small field strengths, at the same time localizing some previously extended states. At higher field strengths, most states become delocalized.

Acknowledgments

The authors are grateful to C. Wilson for useful discussions. This work was supported by a Discovery Grant 2021-03705 from the Natural Sciences and Engineering Research Council of Canada.

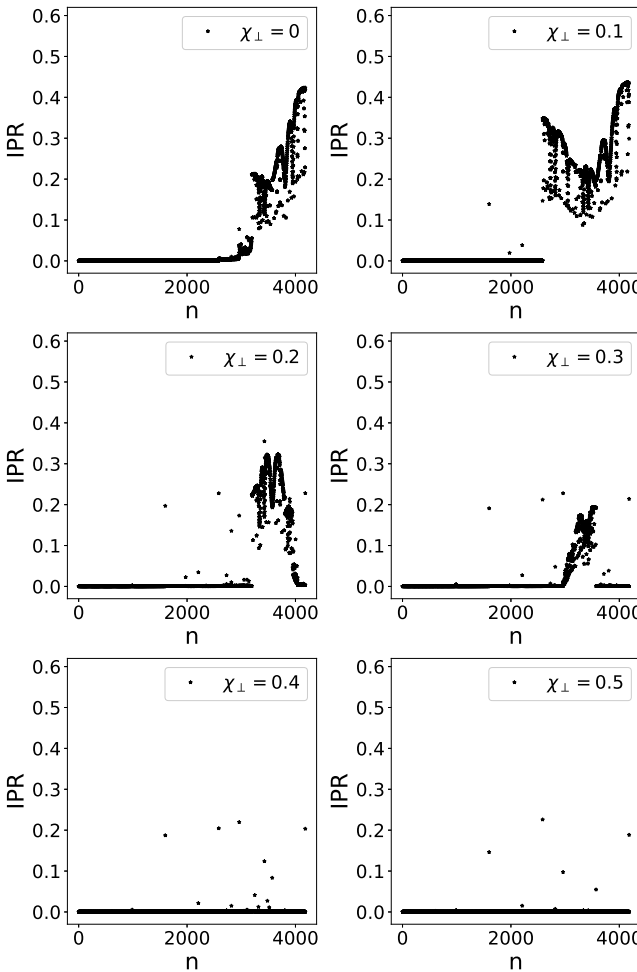


FIG. 10: Values of the IPR as the strength of a perpendicular field χ_{\perp} , as defined in Eq. (13), is increased for $a = 1$ and $d = 0.4$.

Appendix A: “Almost decoupled” chains

In this appendix, all length scales are dimensionless, i.e. measured in the units of the wave function size λ . The wave vectors are also dimensionless, measured in the units of λ^{-1} . External magnetic field is equal to zero.

Let us set the inter-chain separation d to a sufficiently large value, effectively decoupling the chains. As expected, we observe a smooth energy spectrum without gaps, and all values of the IPR become effectively zero. This result is presented in Fig. 11a.

At $d \rightarrow \infty$, the energy spectrum can be calculated analytically. The Hamiltonian (4) takes the form $\hat{H} = \hat{H}_0 = \hat{H}_A + \hat{H}_B$, so that there are two independent families of plane-wave eigenstates:

$$\begin{aligned} |A, k_A\rangle &= \frac{1}{\sqrt{N_A}} (e^{ik_A a}, \dots, e^{ik_A N_A a}, 0, \dots, 0)^\top, \\ |B, k_B\rangle &= \frac{1}{\sqrt{N_B}} (0, \dots, 0, e^{ik_B b}, \dots, e^{ik_B N_B b})^\top, \end{aligned} \quad (\text{A1})$$

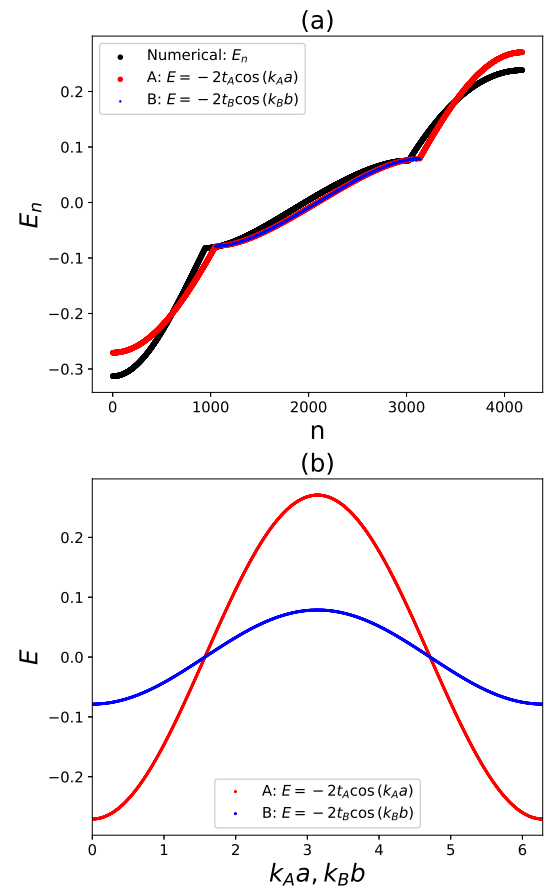


FIG. 11: (Color online) Energy spectra for decoupled chains. (a) Numerical diagonalization of the Hamiltonian (4) for $a = 2$ and $d = 10$. (b) Analytical tight-binding spectrum, Eq. (A3), with $t_A = 0.135$ and $t_B = 0.039$.

where

$$\begin{aligned} k_A &= \frac{2\pi m_A}{N_A a}, \quad 0 \leq m_A \leq N_A - 1, \\ k_B &= \frac{2\pi m_B}{N_B b}, \quad 0 \leq m_B \leq N_B - 1, \end{aligned} \quad (\text{A2})$$

and $N_A a = N_B b = L \gg 1$ is the dimensionless circumference of the chains. In the limit $N_A, N_B \rightarrow \infty$, the wave vectors k_A and k_B corresponding to physically non-equivalent states become quasi-continuous variables limited to the “first Brillouin zones” (BZ): $0 \leq k_A < 2\pi/a$ and $0 \leq k_B < 2\pi/b$.

Although our numerical analysis retains all hopping terms, the ratios of next-nearest to nearest-neighbor hopping are typically quite small (for $a = 2$, they are approximately equal to 0.135 and 0.039 in the A and B chains, respectively), so using the nearest-neighbor approximation in the analytical calculation is well justified. Then, the dispersion relations corresponding to the eigenstates

(A1) take the form

$$E_{A,k_A}^{(0)} = -2t_A \cos(k_A a), \quad E_{B,k_B}^{(0)} = -2t_B \cos(k_B b), \quad (A3)$$

which are plotted in Fig. 11b. When these energy values are ordered from lowest to highest, they closely match the numerical spectrum in Fig. 11a. The two “tail” regions on the left and right sides of Fig. 11a contain only energies corresponding to the A chain while the center region contains to points corresponding to both the A and B chains.

As d is decreased, we treat the effects of the inter-chain coupling perturbatively [52]. The diagonal matrix elements of \hat{H} in the basis (A1) are equal to zero, which means that there are no first order (or any odd order) corrections to the energy levels due to the inter-chain coupling. For even-order corrections we need to know the off-diagonal matrix elements. Using Eqs. (17) and (A2) we obtain:

$$\begin{aligned} \langle A, k_A | \hat{H} | B, k_B \rangle &= \langle B, k_B | \hat{H} | A, k_A \rangle^* \\ &= \frac{1}{\sqrt{N_A N_B}} \sum_{i_A=1}^{N_A} \sum_{j_B=1}^{N_B} e^{-ik_A i_A a} e^{ik_B j_B b} \tilde{t}(i_A, j_B) \\ &= \frac{1}{\sqrt{N_A N_B}} \sum_{\theta_A, \theta_B} e^{-im_A \theta_A} e^{im_B \theta_B} F(\theta_A - \theta_B), \end{aligned} \quad (A4)$$

where $\theta_A = 2\pi i_A / N_A$ and $\theta_B = 2\pi j_B / N_B$ are the angular positions of atoms in the chains, and

$$F(\Theta) = \exp \left[-\sqrt{\left(\frac{L}{\pi} \right)^2 \sin^2 \frac{\Theta}{2} + d^2} \right]$$

is a 2π -periodic function. Representing the latter as a Fourier series, $F(\Theta) = \sum_M F_M e^{iM\Theta}$, and using the identity

$$\sum_{j=1}^N \exp \left[\frac{2\pi i(m-M)}{N} j \right] = N \delta_{m, M \bmod N},$$

we calculate the θ sums in Eq. (A4) and obtain:

$$\begin{aligned} \langle A, k_A | \hat{H} | B, k_B \rangle &= \sqrt{N_A N_B} \sum_M F_M \delta_{m_A, M \bmod N_A} \delta_{m_B, M \bmod N_B}. \end{aligned}$$

Therefore, the matrix elements (A4) are nonzero only if the wave vectors satisfy the condition

$$k_A + \frac{2\pi}{a} n_A = Q = k_B + \frac{2\pi}{b} n_B, \quad (A5)$$

where n_A and n_B are integers, and $Q = 2\pi M / L$. If $n_A = n_B = 0$, then the transitions between the plane-wave states (A1) caused by the inter-chain hopping conserve momentum, i.e. $k_B = k_A$. If either n_A or n_B is nonzero,

then the transitions correspond to “Umklapp” processes, in which k_B is not equal to k_A .

If the incommensurability ratio ρ is irrational, e.g. equal to the golden ratio ϕ , then Eq. (A5) has an infinite number of solutions for k_B at any given k_A . To show this, let us introduce $\nu_A = k_A a / 2\pi$ and $\nu_B = k_B b / 2\pi$, which satisfy $0 \leq \nu_{A,B} < 1$. Then, we obtain from Eq. (A5):

$$Y = \rho X, \quad (A6)$$

where $X = n_A + \nu_A$ and $Y = n_B + \nu_B$. Fixing ν_A and going through all integer values of n_A , one obtains an infinite set of solutions $Y_{n_A}(\nu_A)$ of the above equation. Their fractional parts $\{Y_{n_A}(\nu_A)\}$ give the values of ν_B , while their integer parts correspond to n_B . For finite chains, ρ is equal to N_A / N_B —a ratio of two large coprime numbers. Then, the number of solutions for ν_B of Eq. (A6) is finite and equal to N_B .

Although the number of nonzero matrix elements at given k_A is large or even infinite, their magnitudes, which depend on M and therefore on Q , are expected to decrease rapidly as the Umklapp parameters n_A and n_B increase. These magnitudes are determined by the Fourier coefficients F_M , which are evaluated as follows:

$$\begin{aligned} F_M &= \int_{-\pi}^{\pi} \frac{d\Theta}{2\pi} e^{-iM\Theta} F(\Theta) \\ &\simeq \int_{-\infty}^{\infty} \frac{d\Theta}{2\pi} e^{-iM\Theta} \exp \left[-\sqrt{\left(\frac{L}{2\pi} \right)^2 \Theta^2 + d^2} \right] \\ &= \frac{2d}{L\sqrt{1+Q^2}} K_1 \left(d\sqrt{1+Q^2} \right). \end{aligned}$$

In the second line here we used the fact that at $L \gg 1$ the function $F(\Theta)$ is sharply peaked near $\Theta = 0$, which allows one to replace $\sin(\Theta/2) \rightarrow \Theta/2$ and extend the integration limits to infinities. Then the integral can be calculated analytically [53], with $K_1(x)$ being the modified Bessel function of the second kind. Therefore, we obtain for the matrix elements (A4):

$$\begin{aligned} \langle A, k_A | \hat{H} | B, k_B \rangle &\simeq \frac{2d^2}{\sqrt{ab}} \sum_Q \Phi(Q) \\ &\quad \times \delta_{Q, k_A + 2\pi n_A / a} \delta_{Q, k_B + 2\pi n_B / b}, \end{aligned} \quad (A7)$$

where the function

$$\Phi(Q) = \frac{1}{d\sqrt{1+Q^2}} K_1 \left(d\sqrt{1+Q^2} \right)$$

is plotted in Fig. 12a.

Assuming that the separation between the chains is sufficiently large to make the perturbative treatment of the inter-chain hopping quantitatively valid, one can use the large- x asymptotics $K_1(x) \simeq \sqrt{\pi/2x} e^{-x}$ [54]. The exponential decay of $\Phi(Q)$ means that the matrix elements rapidly decrease as $|Q|$ increases. According to Eq.

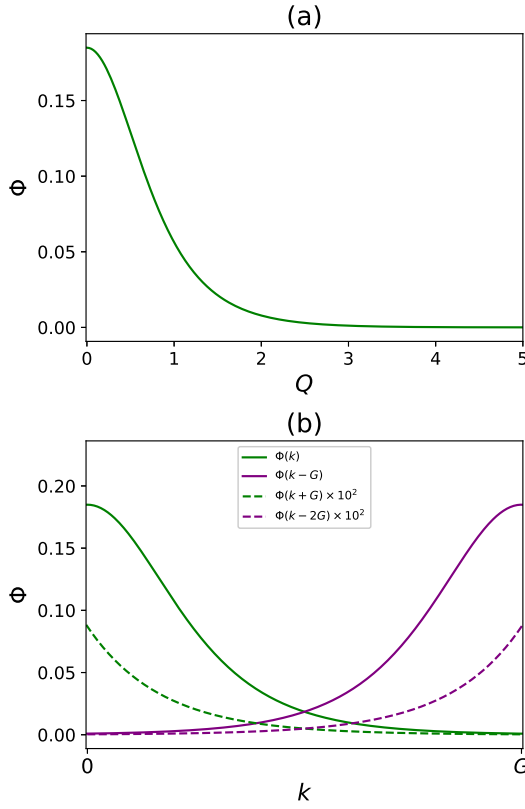


FIG. 12: (Color online) Magnitudes of the inter-chain matrix elements, Eq. (A7), for $d = 1.5$ and $a = 2$. (a) $\Phi(Q)$ decays rapidly as Q increases. (b) $\Phi(k + Gn)$ plotted in the BZ, $0 \leq k < G$. Note the difference in scale between the largest ($n = 0, -1$) and next-largest ($n = 1, -2$) matrix elements.

(A7), this constrains the possible values of the Umklapp numbers n_A and n_B . Namely, by far the largest matrix elements correspond to $n_A, n_B = 0$ or -1 , and the next largest (and considerably smaller) – to $n_A, n_B = 1$ or -2 . This is illustrated in Fig. 12b, where the magnitudes $\Phi(k + Gn)$ are plotted as functions of momentum k in the BZ $0 \leq k < G$, for different values of n (here $k = k_A$ or k_B , $G = 2\pi/a$ or $2\pi/b$, and $n = n_A$ or n_B).

Substituting $n_A, n_B = 0$ or -1 in the constraint (A5), and using the fact that k_A and k_B are restricted to their respective BZs, it is easy to check that there are only two possibilities:

$$k_A = k_B, \quad (A8)$$

which corresponds to $n_A = n_B = 0$, and

$$k_A - \frac{2\pi}{a} = k_B - \frac{2\pi}{b}, \quad (A9)$$

which corresponds to $n_A = n_B = -1$. For k_A and k_B not satisfying these conditions, the matrix elements (A7) either vanish identically or have a negligibly small magnitude for $d \gtrsim 1$.

We can now calculate the corrections to the A -chain dispersion. The second order correction takes the form

$$E_{A,k_A}^{(2)} = \sum_{k_B} \frac{|\langle A, k_A | \hat{H} | B, k_B \rangle|^2}{E_{A,k_A}^{(0)} - E_{B,k_B}^{(0)}}, \quad (A10)$$

where the possible values of k_B are determined by Eqs. (A8) and (A9). The above expression diverges when the condition

$$E_{A,k_A}^{(0)} = E_{B,k_B}^{(0)} \quad (A11)$$

is satisfied. The locations of these inter-band degeneracies depend on the parameters of the system. For example, for $a = 2$ the solutions of Eq. (A11) with k_A and k_B related through Eq. (A8) or (A9) are given by $k_A^{\text{gap}} a \simeq 1.526, 1.861, 4.422$, and 4.757 . The divergence of $E_{A,k_A}^{(2)}$ at these points indicates that we must turn to the degenerate perturbation theory, in which the degeneracies are removed by splitting the energy bands near the intersection points. These spectral gaps are not visible in Figs. 4 and 5 where the energy levels are arranged from lowest to highest.

The spectral gaps shown in Figs. 4 and 5 originate from the *intra-band* degeneracies. To see this, we bias one chain, say the B chain, by adding a constant on-site potential term to \hat{H}_B . For a sufficiently strong bias, the dispersion relations in the A and B chains no longer overlap and the condition (A11) is never satisfied, yet the gaps persist in the energy spectrum according to our numerical results. To capture this effect, we must include the next nonzero term in the perturbation theory, namely the fourth-order energy correction. Using the procedure for deriving the higher-order perturbative corrections developed in Refs. [55, 56] we obtain:

$$E_{A,k_A}^{(4)} = \sum_{k'_A \neq k_A} \sum_{k_B, k'_B} \frac{\langle A, k_A | \hat{H} | B, k_B \rangle \langle B, k_B | \hat{H} | A, k'_A \rangle \langle A, k'_A | \hat{H} | B, k'_B \rangle \langle B, k'_B | \hat{H} | A, k_A \rangle}{(E_{A,k_A}^{(0)} - E_{B,k_B}^{(0)})(E_{A,k_A}^{(0)} - E_{A,k'_A}^{(0)})(E_{A,k_A}^{(0)} - E_{B,k'_B}^{(0)})} - E_{A,k_A}^{(2)} \sum_{k_B} \frac{|\langle A, k_A | \hat{H} | B, k_B \rangle|^2}{(E_{A,k_A}^{(0)} - E_{B,k_B}^{(0)})^2}. \quad (A12)$$

In addition to the already detected inter-chain degeneracies described by Eq. (A11), which are removed by biasing the B chain, the denominator in the first term vanishes when the condition

$$E_{A,k_A}^{(0)} = E_{A,k'_A}^{(0)} \quad (\text{A13})$$

is satisfied for $k'_A \neq k_A$. In Eq. (A12), the values of k_B , k'_A , and k'_B at given k_A allowed by the conditions (A8) and (A9) are given by

$$\begin{aligned} k_B &= k_A, \quad k_A - \frac{2\pi}{a} + \frac{2\pi}{b}, \\ k'_A &= k_A, \quad k_A - \frac{2\pi}{a} + \frac{2\pi}{b}, \quad k_A + \frac{2\pi}{a} - \frac{2\pi}{b}, \\ k'_B &= k_A, \quad k_A - \frac{2\pi}{a} + \frac{2\pi}{b}. \end{aligned} \quad (\text{A14})$$

It is easy to check that for other values of k'_B one cannot complete the closed-loop virtual hopping sequence

$$|A, k_A\rangle \rightarrow |B, k_B\rangle \rightarrow |A, k'_A\rangle \rightarrow |B, k'_B\rangle \rightarrow |A, k_A\rangle,$$

as enforced by the chain of matrix elements in the first term of Eq. (A12).

According to Eqs. (A13), (A3), and (A14), gaps in the spectrum may open up at the wave vectors satisfying the following equation:

$$\cos(k_A a) = \cos\left(k_A a + 2\pi n_1 + \frac{2\pi a}{b} n_2\right),$$

where $(n_1, n_2) = (1, -1)$ or $(-1, 1)$. The solutions have the form $k_A^{\text{gap}} = -(\pi/b)n_2 + (\pi/a)\ell$, where ℓ is an integer. Finally, using Eq. (1) we obtain for the energy gap locations in the BZ:

$$\frac{k_A^{\text{gap}} a}{2\pi} = \frac{1}{2} - \frac{1}{2\rho}, \quad \frac{1}{2\rho}, \quad 1 - \frac{1}{2\rho}, \quad \frac{1}{2} + \frac{1}{2\rho}. \quad (\text{A15})$$

Thus there are two pairs of gaps located symmetrically about the center of the spectrum, the “outer” ones corresponding to the first and fourth values of k_A^{gap} above, and the “inner” ones corresponding to the second and third values of k_A^{gap} . It should be noted that this method does not provide the energy gap width, but merely indicates where in momentum space a gap may occur due to the failure of non-degenerate perturbation theory in the fourth order.

In our numerical analysis in Sec. IV, the eigenvalues

are ordered from lowest to highest according to an integer index n . To compare the gap structure predicted by perturbation theory applied to the spectrum (A3) with these numerical results, we arrange the perturbed spectrum in the same manner. The gaps in momentum space given by (A15) appear symmetrically about the center of the spectrum, which means that each state in the ordered spectrum actually corresponds to two states in the original spectrum. It follows from Eqs. (A2) and (1) that

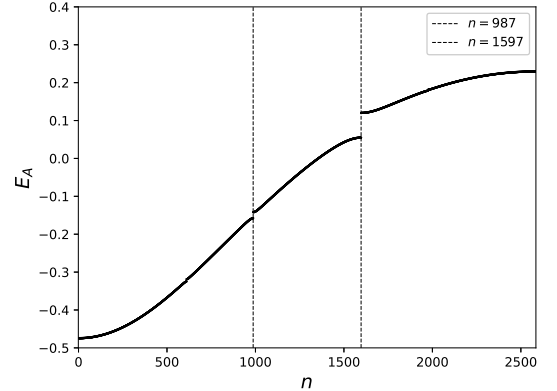


FIG. 13: Numerical spectrum of Eq. (14) for $a = 2$ and $d = 1$, showing only the A -chain band modified by coupling to the B chain. The part corresponding to the modified B -chain band is shifted to higher energies by a strong uniform potential and is not shown. The black dashed lines mark the gap locations predicted by Eq. (A13).

the number of states with energies below the outer gaps is equal to $N_A - N_B$, while the number of states with energies below the inner gaps is equal to N_B . These numbers give the locations of the gaps in the ordered spectrum at indices

$$n = N_A - N_B, \quad N_B. \quad (\text{A16})$$

Substituting here our values for N_A and N_B , we find gaps located at $n = 987$ and 1597 . This prediction agrees exactly with our numerical results in the case where the B chain is biased such that $E_{B,k_B}^{(0)} \gg E_{A,k_A}^{(0)}$. The lower part of the spectrum corresponding to the A -chain dispersion modified by the coupling to the B chain is displayed in Fig. 13. The upper part of the spectrum, which originates from the biased B chain, is pushed up to higher energies and is not shown.

[1] F. Bloch, *Zeitschrift für Physik* **52**, 555 (1929).
[2] P. W. Anderson, *Phys. Rev.* **109**, 1492 (1958).
[3] P. A. Lee and T. V. Ramakrishnan, *Rev. Mod. Phys.* **57**, 287 (1985).
[4] B. Kramer and A. MacKinnon, *Reports on Progress in Physics* **56**, 1469 (1993).
[5] N. W. Ashcroft and N. D. Mermin, *Solid State Physics* (Holt, Rinehart and Winston, 1976).
[6] C. Kittel, *Introduction to Solid State Physics*, 8th ed. (Wiley, New York, 2004).
[7] N. Mott and W. Twose, *Advances in Physics* **10**, 107 (1961).

[8] A. Mackinnon and B. Kramer, Zeitschrift für Physik B Condensed Matter **53**, 1 (1983).

[9] D. J. Thouless, Journal of Physics C: Solid State Physics **5**, 77 (1972) [ps://doi.org/10.1143/JPSJ.56.1470](https://doi.org/10.1143/JPSJ.56.1470).

[10] B. Kramer and A. MacKinnon, Reports on Progress in Physics **56**, 1469 (1993).

[11] J. Billy, V. Josse, Z. Zuo, A. Bernard, B. Hambrecht, P. Lugan, D. Clément, L. Sanchez-Palencia, P. Bouyer, and A. Aspect, Nature **453**, 891 (2008).

[12] T. Schwartz, G. Bartal, S. Fishman, and M. Segev, Nature **446**, 52 (2007).

[13] G. Bergmann, Physics Reports **107**, 1 (1984).

[14] T. Ando, Phys. Rev. B **40**, 5325 (1989).

[15] S. Aubry and G. André, Proceedings, VIII International Colloquium on Group-Theoretical Methods in Physics **3** (1980).

[16] J. Sokoloff, Physics Reports **126**, 189 (1985).

[17] G. A. Domínguez-Castro and R. Paredes, European Journal of Physics **40**, 045403 (2019).

[18] P. G. Harper, Proc. Roy. Soc. Lond. A **68**, 874 (1955).

[19] G. Roati, C. D'Errico, L. Fallani, M. Fattori, C. Fort, M. Zaccanti, G. Modugno, M. Modugno, and M. Inguscio, Nature **453**, 895 (2008).

[20] M. Schreiber, S. Hodgman, P. Bordia, H. Lüschen, M. Fischer, R. Vosk, E. Altman, U. Schneider, and I. Bloch, Science **349**, 842 (2015).

[21] C. M. Soukoulis and E. N. Economou, Phys. Rev. Lett. **48**, 1043 (1982).

[22] S. Das Sarma, S. He, and X. C. Xie, Phys. Rev. Lett. **61**, 2144 (1988).

[23] J. Biddle, B. Wang, D. J. Priour, and S. Das Sarma, Phys. Rev. A **80**, 021603 (2009).

[24] J. Biddle and S. Das Sarma, Phys. Rev. Lett. **104**, 070601 (2010).

[25] F. Liu, S. Ghosh, and Y. D. Chong, Phys. Rev. B **91**, 014108 (2015).

[26] J. C. C. Cestari, A. Foerster, and M. A. Gusmão, Phys. Rev. B **93**, 205441 (2016).

[27] T. Liu and H. Guo, Phys. Rev. B **98**, 104201 (2018).

[28] Y. Wang, X. Xia, L. Zhang, H. Yao, S. Chen, J. You, Q. Zhou, and X.-J. Liu, Phys. Rev. Lett. **125**, 196604 (2020).

[29] D. Vu and S. Das Sarma, Phys. Rev. B **107**, 224206 (2023).

[30] H. P. Lüschen, S. Scherg, T. Kohlert, M. Schreiber, P. Bordia, X. Li, S. Das Sarma, and I. Bloch, Phys. Rev. Lett. **120**, 160404 (2018).

[31] M. Kohmoto and J. R. Banavar, Phys. Rev. B **34**, 563 (1986).

[32] M. Fujita and K. Machida, Journal of the Physical Society of Japan **56**, 1470 (1987), [ps://doi.org/10.1143/JPSJ.56.1470](https://doi.org/10.1143/JPSJ.56.1470).

[33] M. Kohmoto, B. Sutherland, and C. Tang, Phys. Rev. B **35**, 1020 (1987).

[34] A. Jagannathan, Rev. Mod. Phys. **93**, 045001 (2021).

[35] Y. E. Kraus and O. Zilberberg, Phys. Rev. Lett. **109**, 116404 (2012).

[36] A.-M. Guo, X. C. Xie, and Q.-f. Sun, Phys. Rev. B **89**, 075434 (2014).

[37] M. Rossignolo and L. Dell'Anna, Phys. Rev. B **99**, 054211 (2019).

[38] R. Wang, X. M. Yang, and Z. Song, Journal of Physics: Condensed Matter **33**, 365403 (2021).

[39] X. Lin, X. Chen, G.-C. Guo, and M. Gong, Phys. Rev. B **108**, 174206 (2023).

[40] S. Aghtouman and M. V. Hosseini, Scientific Reports **14**, 8782 (2024).

[41] R. J. Bell and P. Dean, Discussions of the Faraday Society **50**, 55 (1970).

[42] D. Thouless, Physics Reports **13**, 93 (1974).

[43] F. Wegner, Z. Phys. B - Condensed Matter **36**, 209 (1980).

[44] M. Y. Azbel, Phys. Rev. Lett. **43**, 1954 (1979).

[45] J. B. Sokoloff, Phys. Rev. B **23**, 6422 (1981).

[46] A. Y. Khinchin, *Continued Fractions* (University of Chicago Press, Chicago, 1964).

[47] S. Carr, D. Massatt, M. Luskin, and E. Kaxiras, Phys. Rev. Res. **2**, 033162 (2020).

[48] D. R. Hofstadter, Phys. Rev. B **14**, 2239 (1976).

[49] M. P. Marder, *Condensed Matter Physics*, 2nd ed. (Wiley, Hoboken, NJ, 2010) Chap. 25.

[50] S. Simon, *The Oxford Solid State Basics* (Oxford University Press, Oxford, 2013).

[51] A. P. Siebesma and L. Pietronero, Europhysics Letters **4**, 597 (1987).

[52] J. J. Sakurai and J. Napolitano, *Modern Quantum Mechanics*, 2nd ed. (Addison-Wesley, San Francisco, 2011).

[53] I. S. Gradshteyn and I. M. Ryzhik, *Tables of Integrals, Series, and Products*, 6th ed. (Academic Press, San Diego, 2000).

[54] M. Abramowitz and I. A. Stegun, eds., *Handbook of Mathematical Functions* (Dover Publications, New York, 1970).

[55] R. Huby, Proceedings of the Physical Society **78**, 529 (1961).

[56] H. J. Silverstone and T. T. Holloway, The Journal of Chemical Physics **52**, 1472 (1970).